Gradient Steepness Influences the Pathfinding Decisions of Neuronal Growth Cones *In Vivo*

Carolyn M. Isbister,[1,3] Paul J. Mackenzie,[3] Kenneth C. W. To,[3] and Timothy P. O'Connor[1,2,3]

Departments of [1]Anatomy and [2]Zoology and [3]Graduate Program in Neuroscience, University of British Columbia, Vancouver, British Columbia, Canada V6T 1Z3

Gradients of chemotropic molecules are generally thought to be fundamental for the guidance of neuronal growth cones in the developing embryo. Here we show that the grasshopper-secreted semaphorin Sema 2a is expressed in a gradient during the period of tibial Ti1 pioneer axon pathfinding into the CNS. At two critical Ti1 growth cone choice points, the Sema 2a gradient differs in steepness, whereas the absolute concentration is the same. Although Ti1 growth cones enter and extend up both steep and shallow gradients of Sema 2a, fewer projection errors occur along the steep gradient, suggesting that the steepness of the gradient encodes the critical guidance information into the pathfinding growth cone. In contrast, an increase in the absolute concentration of Sema 2a appears to constrain the Ti1 growth cone size. Using these *in vivo* gradients, we provide evidence that the Ti1 growth cone detects the Sema 2a gradient by measuring the fractional change in Sema 2a concentration, thereby demonstrating one mechanism that neuronal growth cones may use to detect and read gradients *in vivo*.

Key words: **gradient; axonal guidance; growth cone; semaphorins; chemorepulsion; grasshopper**

Introduction

Since Ramon y Cajal first described the neuronal growth cone over a century ago (Ramon y Cajal, 1937), it has been proposed that spatial gradients of axon guidance molecules provide directional information to pathfinding growth cones. However, it was not until after Gundersen and Barrett (1979) demonstrated that sensory neurons respond to gradients of nerve growth factor *in vitro* that extensive research was directed toward the search for candidate diffusible growth cone guidance signals. Over the past 20 years, many studies have demonstrated that neuronal growth cones can be guided by both diffusible chemoattractants and chemorepellents *in vitro* (Lumsden and Davies, 1983; Tessier-Lavigne et al., 1988; Baier and Bonhoeffer, 1992; Fitzgerald et al., 1993; Pini, 1993; Kennedy et al., 1994; Messersmith et al., 1995, Ming et al., 2002). These *in vitro* chemotropic studies have coevolved with the search for such molecular gradients *in vivo*. However, to date only a few examples of gradient distribution of guidance molecules during periods of axon outgrowth have been documented (Norbeck et al., 1992; Seaver et al., 1996; Braisted et al., 1997; Monschau et al., 1997; Isbister et al., 1999). Although considerable effort has been directed at characterizing chemotactic molecules and their receptors, the mechanisms that neuronal growth cones use to detect these gradients remain primarily unknown. Based primarily on non-neuronal chemotactic cells, two possible mechanisms for growth cone detection of small changes in external gradients have been proposed (Walter et al., 1990; Goodhill, 1998; Goodhill and Baier, 1998). These models differ on which aspect of the change in concentration across the growth cone spatial extent is most critical: the absolute change or the fractional change. Distinguishing the mechanism that is used by neuronal growth cones and the role for the magnitude of chemotropic concentration has been limited by the scarcity of functional data on gradients *in vivo*. To explore these issues, we have used the development of the Ti1 pioneer neuron pathway within the grasshopper limb bud as a model system for investigating neuronal growth cone–gradient interactions *in vivo*.

We have established previously that the secreted semaphorin, grasshopper Sema 2a, is a chemorepulsive guidance molecule expressed in the developing limb bud during the period of Ti1 pioneer neuron outgrowth (Isbister et al., 1999). In the present study, we demonstrate that Sema 2a is expressed within the developing grasshopper limb bud in overlapping distal–proximal and dorsoventral gradients. Interestingly, these gradients are exponential in shape but differ in their steepness; at stereotyped decision points it is the steepness of the gradient and not the absolute level of Sema 2a that provides the critical chemorepulsive information to the pathfinding Ti1 pioneer growth cones. Furthermore, we provide evidence that the Ti1 pioneer growth cone detects these gradients by measuring the fractional change in Sema 2a concentration across its spatial extent rather than by detecting the absolute change.

Materials and Methods

Limb fillets, immunocytochemistry, and antibody perturbation experiments. For limb fillet preparations, *Schistocerca gregaria* embryos were dissected and placed anterior side down on a poly-L-lysine-coated coverslip (6 mg/ml). The exposed posterior epithelium of the Ti1 limb bud was cut lengthwise and unrolled flat to reveal the pioneer pathway (O'Connor et al., 1990; Isbister and O'Connor, 1999). A suction pipette was used to remove the mesodermal cells overlying the limb epithelium. Limb fillets and whole-mount preparations were then fixed and stained

Received Dec. 26, 2001; revised Oct. 7, 2002; accepted Oct. 11, 2002.

This work was supported by Canadian Institutes of Health Research Grant MOP-13246 and National Neurotrauma/Rick Hansen Institute Grant 99019 990. T.P.O. is an EJLB research scholar. C.M.I. was supported by a Rick Hansen Institute Studentship. We thank Drs. D. Bentley and G. Goodhill for their helpful discussions and Dr. T. H. Murphy for the generous use of his equipment.

Correspondence should be addressed to Dr. Timothy P. O'Connor, Department of Anatomy, University of British Columbia, Vancouver, British Columbia, Canada V6T 1Z3. E-mail: jimo@interchange.ubc.ca.

 0270-6474/02/220193-●$15.00/0

for Sema 2a, grasshopper laminin, or neurons as described previously (Isbister and O'Connor, 1999; Isbister et al., 1999; Bonner and O'Connor, 2001). For antibody perturbation experiments, the embryos were cultured in the presence of antibodies generated against functional regions of the semaphorin domain as characterized previously (Isbister et al., 1999). Antibody-cultured embryos were compared with control-cultured embryos (media alone and preimmune antibody). The data are presented as a percentage of the abnormal Ti1 pathways observed. For both cultured and noncultured embryos, the Ti1 pathway was scored as abnormal for one or more of the following observed characteristics: reorientation and distal projection of the proximal Ti1 cell body axon; direct projection of the distal Ti1 cell body axon into the distal limb bud tip; dorsal projection of one or both axons for >50 μm; and failure to initiate a single axon, typically characterized by multiple short, randomly oriented projections from the cell body.

Image acquisition and gradient analysis. For wide-field images, fluorescently labeled fillet and whole-mount limbs were illuminated with a Nikon (Tokyo, Japan) 100 W halogen light with the appropriate filter set (Chroma Technology Corp., Brattleboro, VT) and shuttered with a computer-controlled Lambda 10-2 shutter (Sutter Instruments, Novato, CA). Limbs were imaged with a Princeton Instruments (Trenton, NJ) MicroMax CCD camera (Kodak chip KAF 1400; Eastman Kodak, Rochester, NY) and digitized with MetaView Imaging System 3.6 (Universal Imaging Corporation, West Chester, PA). Gradient measurements were taken from the same focal plane as the Ti1 growth cones. The objective depth of field was ~1 μm, well within the depth sampled by the Ti1 Pioneer growth cones (Caudy and Bentley, 1986, Anderson and Tucker, 1988). For comparative purposes, confocal images were collected with a Bio-Rad (Hercules, CA) MRC 600 system attached to a Zeiss (Oberkochen, Germany) Axioskop microscope and a 40 × 1.3 numerical aperture (NA) Zeiss objective or a 25 × 0.8 NA Zeiss objective (laser intensity, 1–10%; confocal pinhole, 3 Bio-Rad units). Serial images along the *z*-axis (*z*-series) were obtained through the entire specimen (step size, 2 μm), and a maximal-intensity projection was used to generate a two-dimensional representation of maximum Sema 2a fluorescence.

To quantify Sema 2a and laminin protein distribution, 15- to 40-μm-wide line scans were taken along both the distal–proximal and dorsoventral axes (MetaView Imaging System 3.6; Universal Imaging Corporation) in limbs from 30 to 33% development. The distal–proximal line scan started at the distal tip of the flattened anterior compartment epithelium and included the region of limb epithelium in which the Ti1 cell bodies were located. The dorsoventral line scan started at the dorsal edge of the flattened epithelium and spanned the trochanter limb segment. Each fluorescence intensity profile was scaled to its maximum intensity, and the relative intensities were plotted against limb position. Relative intensity profiles along the dorsoventral axis were scaled to the maximum intensity within the limb, which occurred within the distal–proximal profile. The position of the Ti1 cell body along the distal–proximal axis was also recorded for each trace.

Dorsoventral profiles were combined and averaged by aligning to the dorsal edge of the limb, whereas distal–proximal intensity profiles were combined and averaged by aligning to the distal limb tip. In addition, we averaged the distal–proximal intensity profiles by aligning to the Ti1 cell bodies; however, the resulting intensity profile and decay constants were not significantly different from the averaged profile aligned to the distal tip (data not shown). Averaged curves were fit with either linear regression or single exponential decay using pClamp (Axon Instruments, Foster City, CA) and Microcal Origin software (Microcal Software Inc., Northampton, MA). For statistical analysis, curve fitting was performed on the individual distal–proximal and dorsoventral plots, and two-tailed unpaired *t* tests were used to compare slopes or decay rates. To confirm that the region distal to the cell bodies is best described by an exponential equation, we fit equations from the distal tip to the distal edge of the cell body range (56 μm) and to the proximal edge of the cell body range (112 μm). As would be predicted for an exponential curve, there was no difference between the τ values for the two plots ($\tau_{0-56\ \mu m} = 20$; $\tau_{0-112\ \mu m} = 20$). However, linear fits resulted in different slopes for the two sections (e.g., $\Delta F_{0-56\ \mu m} = -0.57\ \mu m^{-1}$; $\Delta F_{0-112\ \mu m} = -0.21\ \mu m^{-1}$), thus further verifying that the distal–proximal gradient in the region distal to the Ti1 cell bodies was best fit with a single exponential. The proximal component of the distal–proximal gradient did not fit an exponential.

Measurement of fractional and absolute change in Sema 2a across growth cones. To calculate change in Sema 2a concentration across growth cones interacting with each of the exponential gradients, we calculated the change in Sema 2a intensity across the distance a typical Ti1 growth cone extends along the distal–proximal and dorsoventral gradient (35 ± 4 and 81 ± 6 μm, respectively). Growth cone length and width included filopodia.

Ectopic expression of Sema 2a in intact limbs. To generate S2 cells that express Sema 2a, the full-length grasshopper *Sema 2a* gene (provided by Dr. Alex Kolodkin, Johns Hopkins University, Baltimore, MD) was cloned into a pIZT/V5-His expression vector that expresses green fluorescent protein (GFP) under a different promoter (Invitrogen, San Diego, CA). *Drosophila* S2 cells were transfected with CellFectin (Invitrogen) and stable transfectants were selected using the Zeocin antibiotic (Invitrogen) and confirmed by GFP fluorescence. A control cell line expressing a truncated Sema 2a protein containing only the Ig domain was also generated (V5-Ig Sema 2a).

To examine whether the ectopic presentation of Sema 2a could perturb Ti1 pathfinding, we transplanted Sema 2a-expressing cells into intact grasshopper limbs. Grasshopper embryos at ~32% development were dissected from their eggs and transferred, dorsal side up, into 35 mm Falcon dishes containing coverslips coated with 5 mg/ml poly-L-lysine (Sigma, St. Louis, MO). Both experimental and control cells were transplanted, via a fire-polished micropipette, into the lumen of intact embryonic grasshopper T3 limbs. Embryos were cultured for 24 hr (5% development) in grasshopper culture medium, fixed, and labeled as described previously (Isbister and O'Connor, 1999; Isbister et al., 1999).

Results

Growth cones sample overlapping chemorepulsive gradients

The Ti1 pioneer neurons are the first neurons to establish a projection to the CNS; this projection is stereotyped in terms of both the substrates contacted and the steering decisions made by the growth cones as they migrate (Fig. 1*A*) (for review, see Bentley and O'Connor, 1992). During Ti1 pioneer neuron axonogenesis, the grasshopper-secreted semaphorin Sema 2a is highly expressed in the distal and dorsal limb compartments (Fig. 1*B*); it has been shown to repel axons from extending into these inappropriate regions (Isbister et al., 1999). Preliminary characterization indicated that during the early stages of Ti1 pioneer neuron axonogenesis, Sema 2a is expressed in a gradient manner, with the highest immunoreactivity distally and dorsally. This gradient distribution was coincident with two critical Ti1 growth cone pathfinding decisions: (1) the initial axon extension along the distal–proximal axis and (2) the dorsoventral reorientation within the trochanter. To investigate whether gradients of Sema 2a play a role in directing Ti1 growth cones at these two decision points, we measured the relative intensity of Sema 2a immunofluorescence along the distal–proximal and dorsoventral axes (Fig. 2*A,B*). The line scan for the distal–proximal gradient measurement spanned the Ti1 cell bodies, whereas the line scan for the dorsoventral gradient measurement spanned the trochanter limb segment. Because the Ti1 projection follows a stereotyped projection along these two limb axes (Bentley and O'Connor, 1992), the direction of axonal growth typically varied <5° from the line-scan axis. The Sema 2a protein concentration decreased steadily along both limb axes, with the maximum fluorescence occurring in the distal and dorsal regions (Fig. 2*C,D*). To test for possible variability in thickness and multiple focal planes over the epithelial sheet, we used confocal microscopy to measure fluorescence in a thin optical section in the same limb fillets (Fig. 2*C,D*). Similar gradients were observed when single confocal slices were examined (data not shown). *In vitro* experiments confirmed

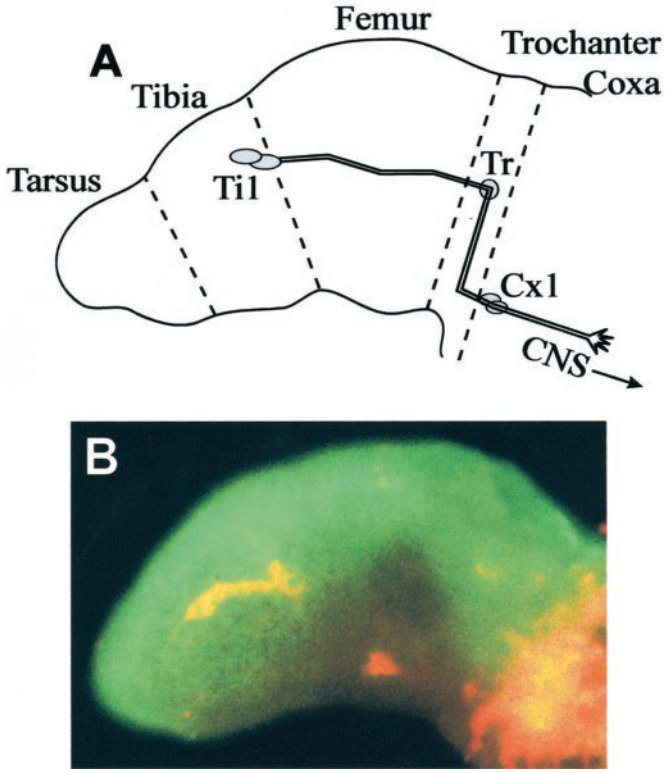

Figure 1. Sema 2a protein distribution during the Ti1 pioneer projection into the CNS. *A*, Drawing of the Ti1 pioneer neuron pathway at ~36% embryonic development. At 29–30% development, the pair of sibling Ti1 pioneer neurons arises from the underlying epithelium. At ~30.5% development, growth cones emerge from their cell bodies and extend axons proximally along the limb axis toward the CNS. Once contact with the Tr neuron has been made (~33% development), the growth cones reorient ventrally along the trochanter epithelium. At ~34% development, the growth cones reorient proximally and exit the trochanter after contact with the Coxa (Cx1) guidepost cells. By 36% development, the Ti1 pioneer growth cones have extended proximally from the Cx1 cells into the CNS. *Dashed lines* signify limb segment boundaries. *B*, Sema 2a distribution (*green*) and neurons (*red*) at 32% development. The Ti1 pioneer growth cones have extended into the mid femur. Distal is to the *left*; dorsal is *up*. Scale bar, 40 μm.

linearity between antibody concentration and fluorescence intensity (Fig. 2*E*). To further verify that the immunofluorescence line-scan analysis accurately reflects protein distribution patterns, we stained developing limb bud fillets for grasshopper laminin, a uniformly expressed basal lamina protein (Bonner and O'Connor, 2001). The average distal–proximal and dorsoventral laminin immunofluorescence plots displayed slopes of near zero (Fig. 2*F*), consistent with the uniform protein distribution. In addition, we have shown previously that the Sema 2a immunofluorescence is indistinguishable from the mRNA expression pattern (Isbister et al., 1999).

The temporal and spatial distribution of Sema 2a protein was highly consistent across 21 limb buds, as illustrated by the average Sema 2a gradient (Fig. 3*A*). Along the distal–proximal axis, the highest distribution was observed in the distal tip, decreasing in a gradient manner toward the proximal limb segment. Curve fit analysis demonstrated that the distal–proximal plot was described by two separate equations, an exponential gradient for the region from the distal limb tip to a point proximal to the cell bodies, followed by a linear gradient more proximal to the cell bodies (Fig. 3*A*, *insets*). Similarly, Sema 2a protein distribution along the dorsoventral axis was highly stereotyped, with the greatest immunoreactivity observed in the dorsal limb and decreasing toward the ventral compartment (Fig. 3*B*). Thus, during the period of axonogenesis and pathfinding, Ti1 pioneer growth cones migrate along both distal–proximal and dorsoventral gradients of Sema 2a.

Ti1 growth cones make two early pathfinding decisions. During the early stages of axonogenesis (30–31% of development), the Ti1 growth cones interact predominantly with the exponential distal–proximal gradient of Sema 2a (see range of cell bodies in Fig. 3*A*). The proximal Ti1 cell body generally projects its growth cone and nascent axon from the proximal pole, whereas the distal Ti1 cell body may initiate its axon near either its proximal or distal pole (Lefcort and Bentley, 1989). Growth cones that emerge from the distal pole typically reorient immediately to extend proximally. Ti1 growth cones make their second major reorientation at 33% development. By this time, Ti1 growth cones have typically contacted the trochanter (Tr) guidepost cell within the trochanter epithelium. Here, the growth cones turn to migrate ventrally within the trochanter down the shallow dorsoventral gradient of Sema 2a, which is now predominant. Therefore, at two critical decision points in the Ti1 pioneer pathway, the Ti1 growth cones migrate down a gradient of Sema 2a.

Steeper gradients provide more chemorepulsion

Interestingly, the exponential component of the distal–proximal Sema 2a gradient was significantly steeper than the exponential gradient along the dorsoventral axis ($\tau = 20$ vs 112 μm; $p < 0.05$; *t* test). The considerable difference in the steepness of the two gradients of Sema 2a at these critical decision points raises the question of whether growth cone guidance information is provided in the gradient steepness. To determine the functional significance of gradient shape, we recorded the frequency of errors that occurs during Ti1 growth cone interaction with the steep distal–proximal gradient and the shallow dorsoventral gradient. In normal developing grasshopper embryos, ~10% of the Ti1 pathways exhibit pathfinding errors (Kolodkin et al., 1992; Isbister et al., 1999). Analysis of untreated embryos at ~36% development revealed that the majority of Ti1 pioneer projection errors occur during growth cone interactions with the shallow dorsoventral Sema 2a gradient, typified by aberrant projections into the dorsal compartment of the limb within or near the trochanter (Figs. 4*B*, 5*A*). We observed few errors during growth cone interaction with the steep exponential distal–proximal gradient of Sema 2a. This skewed distribution of aberrant phenotypes suggests that the steep exponential distal–proximal gradient of Sema 2a confers a greater degree of chemorepulsion to the pathfinding Ti1 growth cones, thus minimizing projection errors. Nevertheless, when errors did occur within the distal–proximal gradient, they were typically either a direct extension of the distal Ti1 cell body axon into the distal tip of the limb bud or a failure to initiate a single axon (Figs. 4*C,D*, 5*A*).

To determine whether the steep distal gradient of Sema 2a is responsible for maintaining the low frequency of projection errors within the distal limb segment, we performed antibody blocking experiments during the period of Ti1 pioneer neuron axonogenesis and outgrowth. A 10-fold increase in Ti1 pioneer projection abnormalities was observed after blocking Sema 2a function. Thus, although it is clear that the distribution of cytoskeletal elements is important for initial axonogenesis (Lefcort and Bentley, 1989) and that many guidance cues influence the Ti1 pioneer projection (Bentley and O'Connor, 1992; Isbister and O'Connor, 2000), the importance of the Sema 2a gradient for establishing the Ti1 pioneer projection is demonstrated by the profound pathfinding errors exhibited after perturbation of the Sema 2a function. Importantly,

the skewed distribution of error subtypes disappeared when Sema 2a function was blocked; with distal projection errors and multiple short axon projection errors occurring as frequently as dorsal projection errors (Fig. 5*C*) ($p = 0.20$; *t* test). These results support the hypothesis that it is the steep gradient of Sema 2a that critically influences the projection of the Ti1 pioneer axons in the proximal direction.

Although the greater degree of distal–proximal chemorepulsion could be conveyed by the steepness of the gradient, an alternative explanation for decreased errors into the distal tip could be higher absolute levels of Sema 2a protein. In addition to a steeper gradient of Sema 2a in the distal limb segment, the levels of Sema 2a protein immunoreactivity in this region were higher than observed elsewhere in the limb. On average, over the distalmost ~20 μm of the limb tip, Sema 2a immunoreactivity sharply rises to levels 20% above the maximum levels observed in the dorsal limb compartment (Fig. 3*A*). Furthermore, by assaying embryos at 36% development, our results may have preferentially selected for errors that occur later in the Ti1 projection, such as those in the dorsal trochanter. Projection errors into the distal tip would not be recorded at 36% if the growth cones had subsequently reoriented to migrate proximally. Therefore, to establish whether absolute levels of chemorepulsion minimize projection errors into the distal tip, we examined axon projection errors at earlier stages of Ti1 outgrowth. It has been observed previously that the dorsal limb compartment is a region the Ti1 growth cones extensively sample and into which they frequently extend erroneous axons before committing to a ventral turn (Caudy and Bentley, 1986; O'Connor et al., 1990; Isbister et al., 1999; Isbister and O'Connor, 2000). Given that the levels of Sema 2a in the 30 μm region distal to the Ti1 cell bodies are similar to the levels observed in the dorsal limb compartment, we predicted that at earlier stages of development the frequency of projections into the region 30 μm distal to the cell bodies would be similar to the frequency of projections into the dorsal limb compartment. However, analysis of axon projection errors at earlier stages of Ti1 outgrowth did not reveal an increase in the frequency of Ti1 axon aberrant projections into the distal tip (Fig. 5*B*). A skewed distribution of error subtypes was evident even at early stages, with extensions into the dorsal limb compartment comprising the majority of axon misprojections. In contrast, distally emerging growth cones (particularly from the distal Ti1 cell body) reoriented on contact with the steeper gradient within the region 30 μm distal to the cell bodies. In this region, the absolute concentration is the same as the dorsal region of the limb fillet into which growth cones frequently misproject, whereas the Sema 2a gradients differ in steepness. These results suggest that it is the steepness of the exponential distal–proximal Sema 2a gradient that conveys the higher degree of chemorepulsion to the pathfinding Ti1 growth cone.

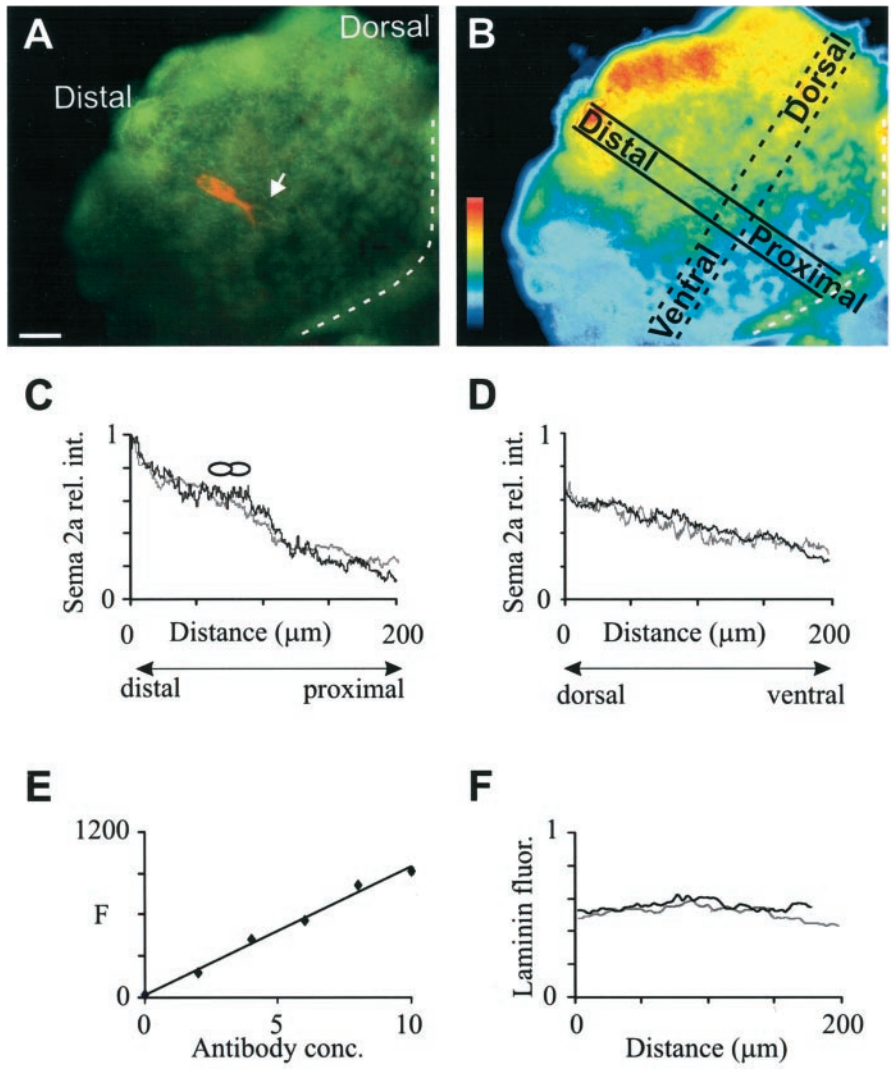

Figure 2. Analysis of Sema 2a gradient. *A*, A representative wide-field image of a double-labeled limb fillet at ~31% embryonic development. The Ti1 growth cones (*arrow*) have just emerged from their cell bodies and are extending toward the trochanter. The *dashed line* denotes the proximal boundary of the filleted limb. *B*, A pseudocolored image of the same fillet shown in *A*, illustrating the orientation of the distal–proximal and dorsoventral line scans. *C*, Distal–proximal gradient: relative intensity (*rel. int.*) profiles of Sema 2a immunoreactivity. The same limb fillet was imaged with wide-field (*gray line*) and confocal (*black line*) microscopy. The location of the cell bodies is denoted by *ovals*. *D*, Dorsoventral axis: relative intensity profiles of Sema 2a immunoreactivity. The same limb fillet was imaged using wide-field (*gray line*) and confocal (*black line*) microscopy. *E*, Linear relationship between fluorescence intensity [arbitrary fluorescence units (*F*)] and fluorescent antibody concentration (in microliters per milliliter). *F*, Intensity profile of laminin immunoreactivity along the distal–proximal axis (*gray line*) and the dorsoventral axis (*black line*), scaled to Sema 2a fluorescence intensity. Scale bar, 30 μm.

To further confirm a role of Sema 2a in guiding the Ti1 pioneer neurons as they extended into the CNS, we tested whether the ectopic presentation of Sema 2a ventrally in the limb would perturb the normal ventral turn made by the Ti1 growth cones in the trochanter. *Drosophila* S2 cells stably transfected with a V5-tagged *Sema 2a* (V5-Sema 2a) (Fig. 6*A*,*B*) were transplanted into intact limbs at ~32–33% development (Fig. 6*C*,*D*). GFP-expressing cells were readily identifiable, and although the expression of V5-Sema 2a was evident, it appeared that the majority of V5-Sema 2a did not diffuse far from the S2 cells (Fig. 6*C*,*D*). Similarly, endogenous Sema 2a appears not to diffuse far from its site of expression (Isbister et al., 1999). Transplants of V5-Sema

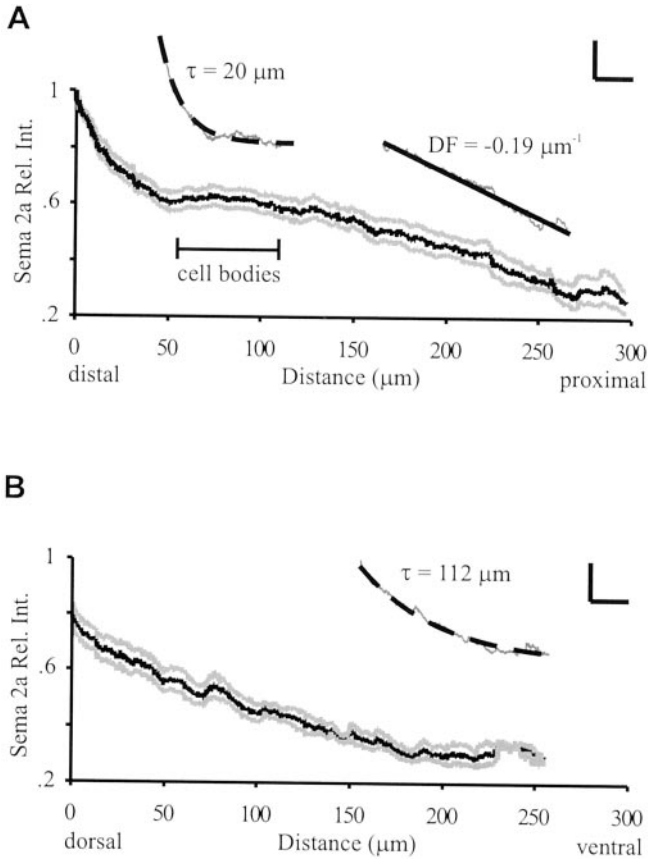

Figure 3. The Sema 2a gradient decayed along both the distal–proximal and dorsoventral limb axes. *A*, Average relative intensity (*Rel. Int.*) profile of Sema 2a immunoreactivity along the distal–proximal axis (average, *black lines*; SEM, *gray lines*). Maximum protein immunoreactivity was observed in the distal tip. For the 21 limbs, the sibling Ti1 cell bodies were located proximally within 56–112 μm from the distal limb tip as indicated. *Inset*, Curve fit analysis indicated that the distal–proximal gradient of Sema 2a was described by a single exponential gradient (decay constant, $\tau = 20$ μm) starting at the distal tip and extending past the proximal edge of the Ti1 cell body range. *DF* indicates the slope of the proximal portion of the Sema 2a gradient. *B*, Average relative intensity profile of Sema 2a distribution along the dorsoventral axis (average, *black*; SEM, *gray*). Sema 2a distribution was maximal dorsally; however, this value was only 79% of the maximum observed along the distal–proximal gradient. *Inset*, The dorsoventral gradient was best described by a single exponential with a decay constant (τ) of 112 μm. Scale bars: for *insets*, *y*-axis, 0.20 U of relative intensity; *x*-axis, 50 μm. $n = 21$ limb fillets.

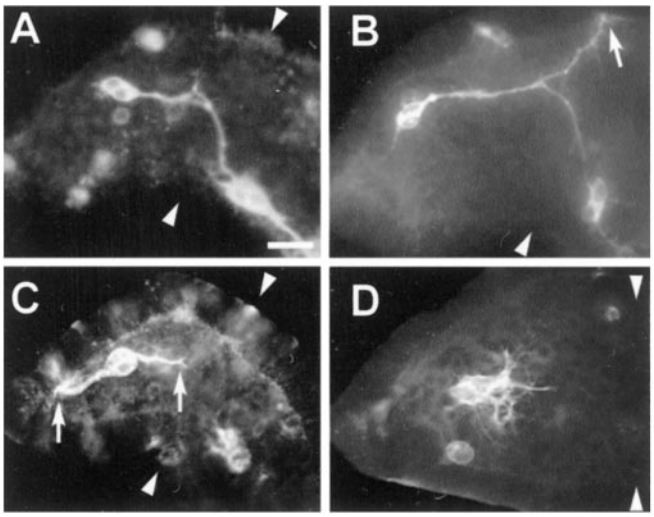

Figure 4. Ti1 pioneer growth cones occasionally misproject up the chemorepulsive gradients of Sema 2a. *A*, A representative example of the Ti1 pioneer projection into the CNS. *B*, A representative example of the dorsal projection error phenotype. The *arrow* denotes the misguided Ti1 pioneer growth cone migrating within the dorsal trochanter; the sibling Ti1 growth cone has successfully completed its projection into the CNS. *C*, A representative example of the distal projection error phenotype. These errors were typically direct projections of the distal Ti1 cell body axon into the extreme distal tip of the limb bud. Although it is not unusual for the distal neuron to initiate an axon at its distal pole (Lefcort and Bentley, 1989), it typically reorients its axon to grow proximally. *Arrows* denote proximal and distal projecting growth cones of the sibling Ti1 cell bodies. *D*, A representative example involving the failure to extend a single axon (termed the multiple short axon phenotype). Typically, the Ti1 pioneer cell bodies displayed multiple short axons projecting radially from around the cell body periphery. We interpret this phenotype as a guidance error, because normally when Ti1 neurons initiate several axons, most of them retract after extending a short distance proximally along the epithelium (O'Connor et al., 1990); however, it cannot be ruled out that this phenotype may indicate a role for Sema 2a in axonogenesis as well as pathfinding. *A–D*, *Arrowheads* denote the trochanter limb segment. Scale bar: *A*, *B*, 60 μm; *C*, *D*, 50 μm.

2a-expressing S2 cells into the ventral limb compartment resulted in perturbed Ti1 axon turning at the trochanter limb segment in the majority of limbs (75% exhibited errors; $n = 40$) (Fig. 6*E–J*). Typically axons did not turn ventrally (Fig. 6*E–G*) or did not complete the ventral turn, often turning dorsally again (Fig. 6*H–J*). Control cells expressing a truncated Sema 2a, containing only the Ig domain, had little effect on Ti1 pathfinding (17% errors; $n = 17$) (Fig. 6*K–M*). Similarly, V5-Sema 2a-expressing cells restricted to the dorsal compartment of the limb had little effect on Ti1 pathfinding (data not shown), suggesting that the addition of Sema 2a in regions of high expression did not disrupt the information imparted by the endogenous gradient. These observations provide additional support for the role of Sema 2a as a critical guidance cue in the Ti1 projection.

Absolute levels of chemorepellent may constrain growth cone size

An alternative explanation for the increased chemorepulsion conferred by the distal–proximal gradient of Sema 2a is that the growth cones migrating within this gradient are exposed to more total repellent. Although the levels surrounding the cell bodies are similar to the levels of Sema 2a in the dorsalmost region of the trochanter, normally only a small number of the filopodia appear to extend into this dorsalmost region of high Sema 2a immunoreactivity. In contrast, during migration within the steep distal–proximal gradient, high levels of Sema 2a surround the entire growth cone surface. Therefore, it could be argued that the absolute level of repellent may be responsible for the decreased frequency of erroneous projections into the distal limb.

To test whether absolute Sema 2a concentration sampled over the growth cone contributes to the difference in error frequency, we calculated the total amount of Sema 2a encountered by the Ti1 growth cones at the two pathfinding decision points: where the growth cones emerge from the cell bodies and extend proximally within the femur and where the growth cones reorient and turn ventrally within the trochanter. To calculate the area of limb epithelium sampled by a typical Ti1 growth cone, we measured the average growth cone length and width (including filopodia) at these two decision points. Growth cones extended 35 ± 4 μm along the distal–proximal axis, with a width of 31 ± 4 μm at the first decision point, for a surface area of 1085 μm^2 ($n = 12$). At the second decision point, growth cones extended $81 \pm 6 \times 26 \pm 1$ μm, for a surface area of 2106 μm^2 ($n = 18$). The total amount of Sema 2a sampled by the Ti1 growth cone was calculated by multi-

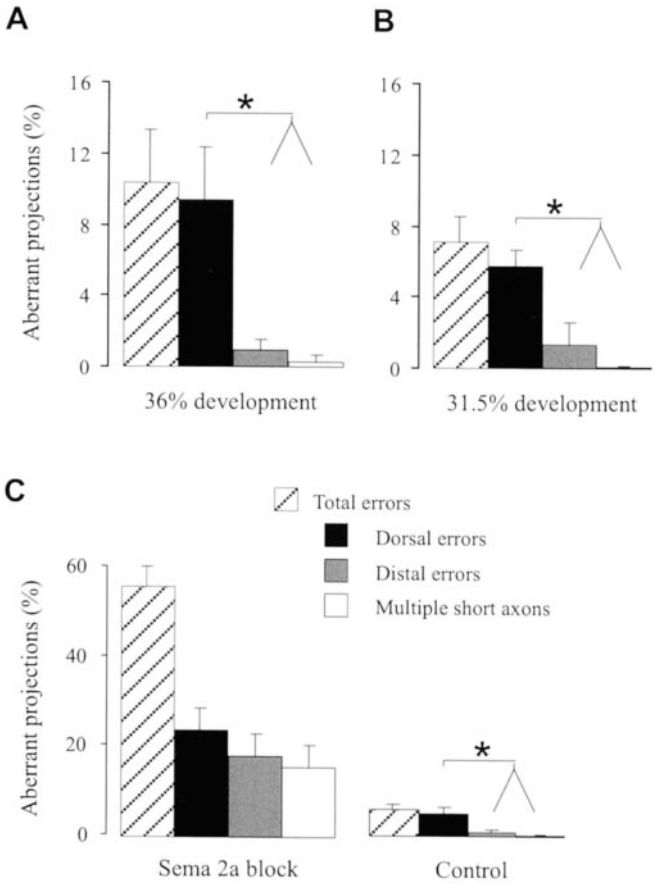

Figure 5. Steep distal–proximal gradient of Sema 2a ensures Ti1 pioneer axonogenesis and proximal outgrowth. *A*, In untreated embryos, the majority of projection errors occurred within the dorsoventral Sema 2a gradient, resulting in a skewed distribution of error phenotypes. Data from eight experiments, $n = 197$. *B*, A skewed distribution of error phenotypes in untreated embryos was observed early in axon outgrowth (~31.5% development). Data from four experiments, $n = 106$. *C*, Increase in total number of axon projection errors and loss of skewed distribution of error phenotypes after functional perturbation of the Sema 2a gradients with antibodies directed against Sema 2a. Data from five experiments, $n = 289$. Embryos cultured with preimmune antibodies (*Control*) exhibit the same skewed distribution of error phenotypes as the untreated embryos (*A, B*). *n* refers to the number of Ti1 projections scored. Error bars indicate SEM. $*p < 0.05$.

plying the growth cone area by averaged relative Sema 2a intensity. Growth cones sampled similar total amounts of Sema 2a at the two decision points (224,034 ± 9803 vs 247,918 ± 16,033 U of relative fluorescence; first and second decision points, respectively; $p > 0.05$; *t* test). A second calculation was performed using values previously published for the Ti1 growth cone sampling area that more closely resembled growth cone morphology (O'Connor et al., 1990), producing similar results (92,938 ± 4067 vs 101,265 ± 6549 U of relative intensity; first and second decision points respectively; $p > 0.05$; *t* test). Thus, the total amount of surround repulsion may regulate growth cone size, allowing the growth cone to expand and branch until the total amount of Sema 2a encountered reaches a critical level that inhibits additional expansion. In addition, the similarity in the total amount of Sema 2a sampled by Ti1 growth cones at the two steering points provides additional evidence that gradient steepness rather than the absolute Sema 2a level confers the critical chemorepulsive guidance information.

Models of growth cone gradient-reading mechanisms *in vivo*

For Sema 2a gradient steepness to confer guidance information, the gradient-reading mechanism used by the Ti1 growth cone must be sensitive enough to detect the difference in steepness between the two gradients. Two models for growth cone detection of small changes in external gradients have been proposed; they differ in whether the absolute change or the fractional change in concentration across the growth cone is most important (Walter et al., 1990; Goodhill, 1998; Goodhill and Baier, 1998; Goodhill and Urbach, 1999). The absolute change model proposes that the growth cone detects an absolute change in ligand concentration (ΔC) across its spatial extent (Fig. 7*A*). In contrast, in the fractional change mechanism, the growth cone measures the change in concentration (ΔC) across its spatial extent as a fraction of the average concentration, *C*, that is detected across the growth cone (Fig. 7*A*). Similar models are under debate in the chemotaxis of cellular slime mold, leukocytes, and other eukaryotic cell types (Berg and Purcell, 1977; Devreotes and Zigmond, 1988; Parent and Devreotes, 1999). To investigate growth cone gradient-reading mechanisms *in vivo*, we took advantage of the large size of the Ti1 growth cones and the well characterized nature of the Ti1 pioneer projection and Sema 2a gradients. For the Ti1 growth cone to use the fractional change mechanism to detect the gradient steepness, it would be expected that the fractional change across a growth cone within the distal–proximal gradient should be significantly higher than the fractional change across a growth cone interacting with the dorsoventral gradient within the trochanter. We applied both the fractional and absolute change model to our *in vivo* gradient data and calculated the change in Sema 2a concentration across the growth cone during interactions with the two gradients. Using the fractional change model, Ti1 growth cones migrating within the steep exponential distal–proximal gradient would detect a greater relative drop in Sema 2a concentration than that detected by growth cones within the shallow dorsoventral gradient (166 vs 71% of average concentration sampled by the growth cone) (Fig. 7*B–D*) ($p < 0.05$; *t* test). The higher fractional change across the growth cone could signal more repulsion and, consequently, could result in fewer erroneous growth cone projections up the distal–proximal chemorepulsive gradient. In contrast, there was no significant difference in the absolute change of Sema 2a across Ti1 growth cones within the two gradients (Fig. 7*B–D*) ($p = 0.15$; *t* test).

Several recent studies in non-neuronal systems have revealed that directional orientation along a gradient of chemoattractant requires asymmetric intracellular signaling to redistribute intracellular components to the leading edge of the cell (Dekker and Segal, 2000; Jin et al., 2000; Sasaki et al., 2000; Servant et al., 2000). For example, external chemotactic gradients cause neutrophils to organize new sites of actin polymerization on the cell surface directed toward the highest concentration of chemoattractant (Weiner et al., 1999). It is possible that a similar spatial regulation of signal transduction and actin polymerization underlies Ti1 growth cone steering events during interaction with the chemorepulsive gradients of Sema 2a. In support of this hypothesis, Ti1 pioneer growth cones in the process of turning ventrally within the trochanter extend ventrally directed filopodia 300% faster than dorsally directed filopodia (Isbister and O'Connor, 1999). Interestingly, these ventrally directed filopodia often overlap with dorsally directed filopodia of the sibling Ti1 pioneer neuron and therefore sample the same environment, only in the opposite direction (Isbister and O'Connor, 2000).

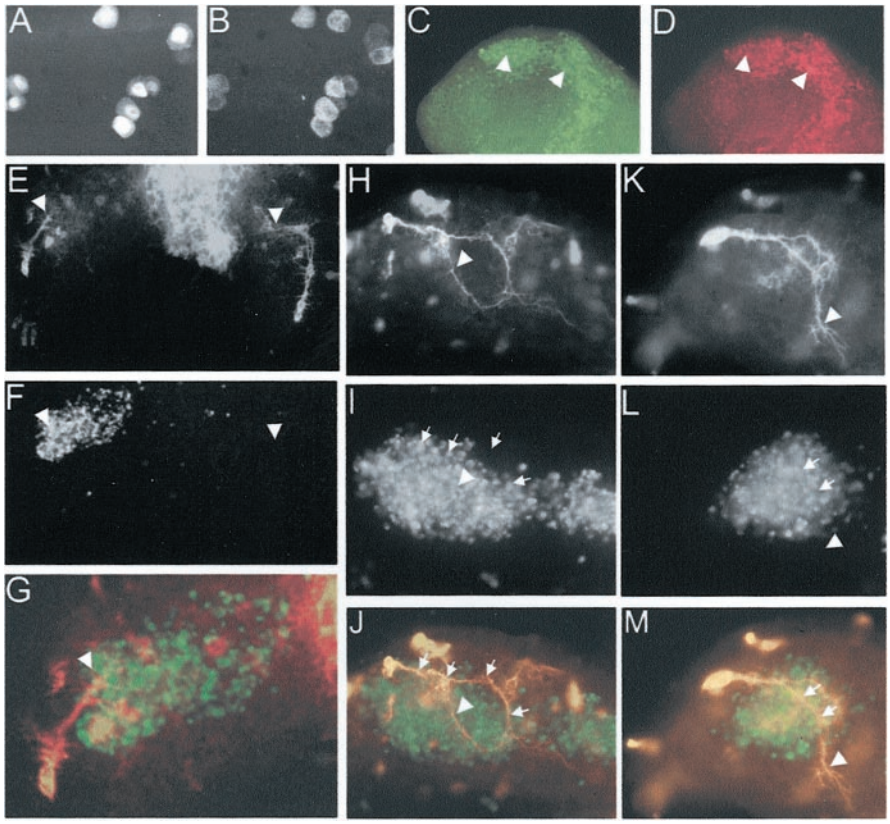

Figure 6. Ectopic expression of recombinant Sema 2a perturbs pathfinding by Ti1 pioneer neurons. *A, B*, GFP and V5-Sema 2a fluorescence, respectively, of transfected S2 cells. Note that the great majority of cells express both GFP and Sema 2a. GFP fluorescence (*C*) and V5-Sema 2a immunofluorescence (*D*) of S2 cells transplanted into a limb bud are shown. Note that, in this example, the majority of cells have been transplanted into the dorsal region of the limb. *E*, Low-magnification image of an experimental (left limb) and a contralateral control limb labeled with anti-HRP immunofluorescence. The growth cone of the experimental limb has not turned ventrally (*arrowhead* in left limb), whereas the growth cone of the contralateral limb (*arrowhead* in right limb) has contacted the Cx cell. The midline fluorescence is the ventral nerve cord (CNS). *F*, Similar image as *E*, showing the transplanted GFP+ V5-Sema 2a-expressing cells in the experimental limb. *Arrowheads* indicate the locations of the experimental and control growth cones. *G*, A higher-magnification overlay image of the experimental limb showing the Ti1 projection (*red*) and the location of the GFP+ V5-Sema 2A cells (*green*). *H*, Anti-HRP immunofluorescence showing a Ti1 pioneer growth cone (*arrowhead*) in an experimental limb that has turned ventrally in the trochanter and then dorsally back toward the midfemur. *I*, The same limb as in *H*, showing the location of the GFP+ V5-Sema 2A cells. Note that the axon traveled along the dorsal margin of the GFP cells before turning ventrally (*arrows*). The *arrowhead* indicates the location of the growth cone. *J*, An overlay image of *H* and *I* showing the Ti1 pathway (*red*) and the GFP+ V5-Sema 2A cells (*green*). *K*, Anti-HRP immunofluorescence showing a Ti1 pioneer growth cone (*arrowhead*) in a control limb that has turned ventrally in the trochanter and has contacted the Cx cell (data not shown). *L*, The same limb as in *K*, showing the location of the control GFP+ V5-Ig Sema 2a cells. The *arrows* indicate the location of the axon, and the *arrowhead* indicates the location of the growth cone. *M*, An overlay image of *K* and *L* showing the Ti1 pathway (*red*) and the GFP+ V5-Ig Sema 2A cells (*green*).

Discussion

Overlapping gradients specify pathfinding decisions

In the present study, we show that grasshopper Ti1 pioneer growth cones migrate down perpendicular gradients of the chemorepulsive secreted semaphorin Sema 2a, thus indicating that overlapping gradients of the same molecule can result in accurate pathfinding. The two repulsive Sema 2a gradients converge near the Tr guidepost cell located in the midtrochanter. Interestingly, this is a position where the Ti1 pioneer growth cones stop and increase their sampling area, apparently searching for the appropriate cue(s) that will eventually reorient the growth cones to migrate ventrally within the trochanter (O'Connor et al., 1990). The shallower dorsoventral chemorepulsive gradient of Sema 2a within the trochanter could provide the necessary chemorepulsion to minimize dorsal projection errors, yet permit growth cone expansion and exploration, thereby increasing the probability of detecting subsequent guidance signals. In contrast, because there would likely be no benefit in exploring the distal tip of the limb bud, a steep gradient of Sema 2a in the distal limb bud could ensure both reliable Ti1 axon initiation and proximal extension. We rarely observed aberrant projections into the ventral limb compartment, suggesting the presence of an attractive cue emanating from the distal and dorsal limb-bud region or, alternatively, a repulsive ventral cue. Similar to other *in vivo* systems, there are most likely additional unidentified guidance molecules expressed within the developing grasshopper limb bud during Ti1 pioneer pathfinding (for review, see Isbister and O'Connor, 2000). However, loss-of-function and gain-of-function experiments often reveal much about the function of a single guidance cue *in vivo* (Mitchell et al., 1996; Serafini et al., 1996; Brown et al., 2000). Similarly, blocking the function or ectopically expressing Sema 2a leads to highly unreliable pathfinding, in which aberrant growth cones often fail to contact the Tr guidepost cell or complete the ventral turn, typically extend into the distal and dorsal limb compartments, and ultimately fail to reach their targets within the CNS. Thus, regardless of additional cues, the perpendicular chemorepulsive gradients of Sema 2a appear critical for the reliable extension of the Ti1 growth cones. Therefore, a characterization of the *in vivo* gradient could lead us to a better appreciation of the critical components necessary for directing neurite growth.

Gradient steepness confers pathfinding information to growth cones

During two key pathfinding decision points along the stereotyped Ti1 pioneer projection, the Ti1 growth cone interacts with gradients of Sema 2a that differ in steepness but are similar in magnitude and sign. Our analysis of the typical Ti1 growth cone pathfinding errors in normal developing grasshopper embryos revealed that the growth cones err more frequently during interaction with the shallow dorsoventral gradient of Sema 2a than during interaction with the steep distal–proximal gradient. Our findings suggest that the higher degree of chemorepulsion exhibited by the distal–proximal Sema 2a gradient is conveyed by the steepness of the gradient and not by the absolute level of protein. Similarly, Brown et al. (2000) have shown that relative repulsive signaling through ephrin receptors, rather than absolute levels, is important for correct retinotectal mapping. Even neurons that had artificially high levels of receptor were able to extend into the tectum and respond appropriately to the graded ephrin expression (Brown et al., 2000).

For a growth cone to use gradient shape for guidance, the

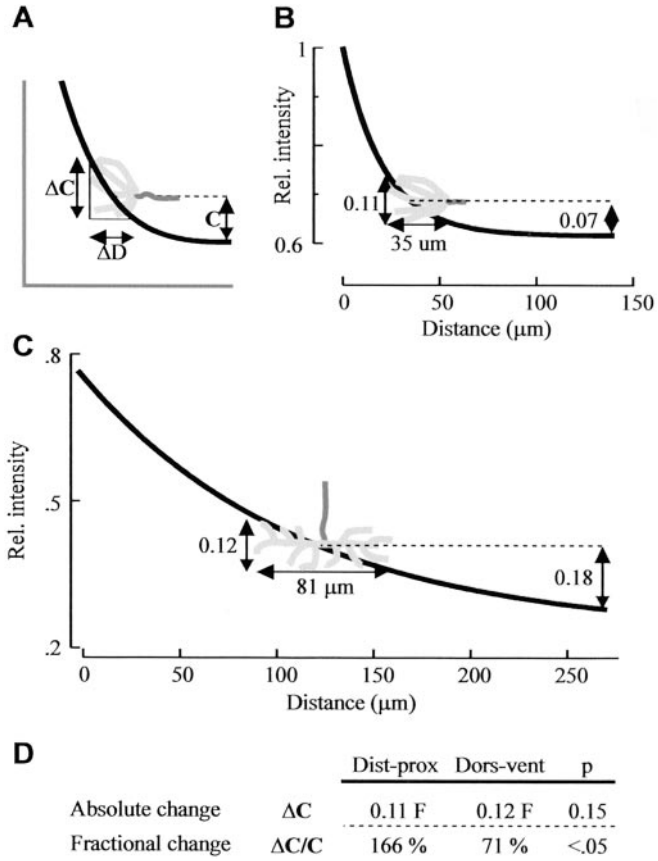

D

		Dist-prox	Dors-vent	p
Absolute change	ΔC	0.11 F	0.12 F	0.15
Fractional change	ΔC/C	166 %	71 %	<.05

Figure 7. Ti1 pioneer growth cones detect the steepness of the Sema 2a gradients using a fractional change mechanism. *A*, Illustration of the fractional change and the absolute change gradient-reading mechanisms. ΔC indicates the absolute change in ligand concentration across the growth cone. *C* indicates the average ligand concentration detected across the growth cone, where 0 is the baseline concentration for the gradient (depicted as a *dashed line*). $\Delta C/C$ indicates the fractional change in ligand concentration across the growth cone. ΔD is the distance the growth cone spans along the gradient. ΔD varies during development, because the Ti1 growth cone expands with proximal migration toward the trochanter. *B*, At 31.5% development, the young Ti1 growth cone (depicted in *gray*) spans an average distance of 35 μm along the distal–proximal gradient. The absolute change (ΔC) equals 0.11 relative intensity (*Rel. intensity*), and the fractional change ($\Delta C/C$) equals 166% of the average concentration sampled by the growth cone. *C*, By 33% development, the growth cone (*gray*) has contacted the Tr guidepost cell within the trochanter and has increased in average size to 81 μm along the dorsoventral gradient. Within the trochanter, the absolute change (ΔC) equals 0.12 relative intensity, and the fractional change ($\Delta C/C$) equals 71%. *D*, Table comparing absolute change and relative change in Sema 2a levels across the typical Ti1 growth cone at the two limb positions. Absolute change in Sema 2a levels across the growth cones is similar at the two decision points ($p = 0.15$; *t* test). In contrast, fractional change in Sema 2a levels across the growth cone is markedly different at the two positions ($p < 0.05$). *Dist-prox*, Distal–proximal; *Dors-vent*, dorsoventral.

growth cone must be capable of detecting spatial differences in guidance cues across its extent. An elegant *in vitro* study by Baier and Bonhoeffer (1992) demonstrated that temporal retinal growth cones could detect small concentration changes of guidance molecules across their spatial extent. By varying the steepness of the repellent gradients in a stripe assay, they showed that the degree of growth cone response correlated with the strength, or steepness, of the gradient. Bagnard et al. (2000) have used defined *in vitro* gradients of chemoattractive and chemorepulsive semaphorins to demonstrate that cortical axon growth cones can reliably read the sign of gradients; however, they found that the cortical axon length was independent of differing gradient absolute concentration or steepness. In contrast, Rosentreter et al. (1998) demonstrated that temporal retinal ganglion cell axons enter and extend up linear gradients of tectal membrane repellents to an avoidance point inversely correlated with the slope (i.e., axon extension is longer within shallower gradients). Notably, the points at which axon extension stopped were not found at a common absolute concentration but rather at a similar increment of concentration over the basal level. Although this study does not address the ability of gradients to induce growth cone turning, these findings are remarkably consistent with our *in vivo* results. We found that Ti1 growth cones extend further up the shallow dorsoventral gradient of Sema 2a compared with the steep distal–proximal gradient. In addition, similar to the cessation of temporal retinal axon extension, the Ti1 growth cones likely turn to migrate down the repulsive gradients after detecting a critical increment, or fractional change, in Sema 2a across their spatial extent rather than an absolute change in concentration (see below). Together, our results indicate that the magnitude and shape of gradients differentially influence neuronal growth cones. The shape, or relative steepness, of the Sema 2a gradient confers the strength of chemorepulsion, whereas the overall amount of Sema 2a encountered by the Ti1 growth cone appears to constrain its size.

Recent work by Ming et al. (2002) has shown that growth cones temporally desensitize and resensitize to gradients of guidance cues *in vitro*, resulting in a pattern of zigzag axonal growth. Although the Ti1 growth cones occasionally branch as they extend along the proximal femur epithelium, they rarely show branching or zigzag growth in the distal femur or after turning ventrally along the trochanter (O'Connor et al., 1990; O'Connor and Bentley, 1993). This difference in growth cone extension *in vivo* may reflect the presence of additional guidance cues, the lack or reduction of desensitization of the Ti1 growth cones to Sema 2a, or the relatively short duration of time required to make a steering decision in the Sema 2a gradient. Although the temporal sensitivity of growth cones to guidance gradients is undoubtedly an important feature of guidance *in vivo*, it is currently unclear whether growth cone desensitization plays a role in detecting the Sema 2a gradient in the grasshopper limb bud.

Models of growth cone gradient-reading mechanisms *in vivo*

We applied our data to two models for the detection of changes in gradients across growth cones: the absolute change and fractional change models (Walter et al., 1990; Goodhill, 1998; Goodhill and Baier, 1998; Goodhill and Urbach, 1999). We found that, because of the difference in growth cone size at the dorsoventral decision point versus the distal–proximal branch point, there was no difference in the absolute change of Sema 2a protein levels across the growth cone at the two locations (Fig. 7). However, differences in the relative concentrations of Sema 2a across the growth cone were apparent, lending support to the suggestion that, in our system, the growth cones use relative changes in protein levels at the two decision regions.

For these calculations, we used a typical growth cone emerging from the distal pole of the distal Ti1 cell body to calculate the change in Sema 2a concentration across a growth cone interacting with the exponential distal–proximal gradient. Given that the proximal Ti1 cell body also sends out an axon, we repeated the fractional and absolute change model calculations for a typical growth cone emerging from the proximal Ti1 cell body. We found that the absolute change mechanism of gradient detection would predict that the distal–proximal gradient actually provides less chemorepulsion to the proximal Ti1 growth cone than the

shallower dorsoventral gradient, a finding inconsistent with the decreased error rate along the distal–proximal axis. Furthermore, although the Ti1 growth cones are emerging on the tail of the steep exponential distal–proximal gradient, a growth cone using the fractional change mechanism of gradient detection would not have to extend far into the distal limb compartment to detect the increasing Sema 2a chemorepulsion, because the fractional change would be constant everywhere along the exponential curve. This may explain why distally emerging Ti1 growth cones reorient immediately without extending into the distal tip. A similar mechanism of gradient detection may be used by the Ti1 cell body to determine the initial site of axon outgrowth.

The large decrease in Sema 2a concentration across the Ti1 growth cone is consistent with the large size of the Ti1 growth cones and the relative steepness of the Sema 2a gradient. Interestingly, the estimated minimum fractional change detectable by a temporal retinal growth cone is predicted to be 1% (Fitzgerald et al., 1993). Although we did not measure the minimum gradient detectable by the Ti1 growth cones, it appears that *in vivo* Ti1 growth cones use considerably steeper gradients of Sema 2a for reliable pathfinding. However, our previous data showing that filopodia that are overlapping but directed in opposite directions extend at different rates (Isbister and O'Connor, 1999) confirm that growth cones, and perhaps even individual filopodia, are capable of detecting and reading gradients across their spatial extent (Isbister and O'Connor, 2000). We speculate that the increased extension rate of ventrally directed filopodia results from preferential localization of actin polymerization sites to the filopodia directed down the dorsoventral chemorepellent gradient (O'Connor and Bentley, 1993; Isbister and O'Connor, 2000). The Ti1 pioneer projection and chemorepulsive gradients of Sema 2a will likely provide a useful model system for additional analysis of neuronal growth cone gradient-reading mechanisms and intracellular responses to chemotropism *in vivo*.

References

Anderson H, Tucker RP (1988) Pioneer neurones use bas lamina as a substratum for outgrowth in the embryonic grasshopper limb. Development 104:601–608.

Bagnard D, Thomasset N, Lohrum M, Püschel A, Bolz J (2000) Spatial distributions of guidance molecules regulate chemorepulsion and chemoattraction of growth cones. J Neurosci 20:1030–1035.

Baier H, Bonhoeffer F (1992) Axon guidance by gradients of a target-derived component. Science 255:472–475.

Bentley D, O'Connor TP (1992) Guidance and steering of peripheral pioneer growth cones in grasshopper embryos. In: The nerve growth cone (Letourneau PC, Kater SB, Macagno ER, eds), pp 265–282. New York: Raven.

Berg HC, Purcell EM (1977) Physics of chemoreception. Biophys J 20:193–219.

Bonner J, O'Connor TP (2001) The permissive cue laminin is essential for growth cone turning *in vivo*. J Neurosci 21:9782–9791.

Braisted JE, McLaughlin T, Wang HU, Friedman GC, Anderson DJ, O'Leary DD (1997) Graded and lamina-specific distributions of ligands of EphB receptor tyrosine kinases in the developing retinotectal system. Dev Biol 191:14–28.

Brown A, Yates PA, Burrola P, Ortuno D, Vaidya A, Jessell TM, Pfaff SL, O'Leary DD, Lemke G (2000) Topographic mapping from the retina to the midbrain is controlled by relative but not absolute levels of EphA receptor signaling. Cell 102:77–88.

Caudy M, Bentley D (1986) Pioneer growth cone steering along a series of neuronal and non-neuronal cues of different affinities. J Neurosci 6:1781–1795.

Dekker LV, Segal AW (2000) Perspectives: signal transduction: signals to move cells. Science 287:982–983.

Devreotes PN, Zigmond SH (1988) Chemotaxis in eukaryotic cells: a focus on leukocytes and Dictyostelium. Annu Rev Cell Biol 4:649–686.

Fitzgerald M, Kwiat GC, Middleton J, Pini A (1993) Ventral spinal cord inhibition of neurite outgrowth from embryonic rat dorsal root ganglia. Development 117:1377–1384.

Goodhill GJ (1998) Mathematical guidance for axons. Trends Neurosci 21:226–231.

Goodhill GJ, Baier H (1998) Axon guidance: stretching gradient to the limit. Neural Comput 10:521–527.

Goodhill GJ, Urbach JS (1999) Theoretical analysis of gradient detection by growth cones. J Neurobiol 41:230–241.

Gundersen RW, Barrett JN (1979) Neuronal chemotaxis: chick dorsal-root axons turn toward high concentrations of nerve growth factor. Science 206:1079–1080.

Isbister CM, O'Connor TP (1999) Filopodial adhesion does not predict growth cone steering events *in vivo*. J Neurosci 19:2589–2600.

Isbister CM, O'Connor TP (2000) Mechanisms of growth cone guidance and motility in the developing grasshopper embryo. J Neurobiol 44:271–280.

Isbister CM, Tsai A, Wong ST, Kolodkin AL, O'Connor TP (1999) Discrete roles for secreted and transmembrane semaphorins in neuronal guidance in vivo. Development 126:2007–2019.

Jin T, Zhang N, Long Y, Parent CA, Devreotes PN (2000) Localization of the G protein $\beta\gamma$ complex in living cells during chemotaxis. Science 287:1034–1036.

Kennedy TE, Serafini T, de la Torre JR, Tessier-Lavigne M (1994) Netrins are diffusible chemotropic factors for commissural axons in the embryonic spinal cord. Cell 78:425–435.

Kolodkin AL, Matthes DJ, O'Connor TP, Patel NH, Admon A, Bentley D, Goodman CS (1992) Fasciclin IV: sequence, expression, and function during growth cone guidance in the grasshopper embryo. Neuron 9:831–845.

Lefcort F, Bentley D (1989) Organization of cytoskeletal elements and organelles preceding growth cone emergence from an identified neuron in situ. J Cell Biol 108:1737–1749.

Lumsden AGS, Davies AM (1983) Earliest sensory nerve fibres are guided to peripheral targets by attractants other than nerve growth factor. Nature 306:786–788.

Messersmith EK, Leonardo ED, Shatz CJ, Tessier-Lavigne M, Goodman CS, Kolodkin AL (1995) Semaphorin III can function as a selective chemorepellent to pattern sensory projection in the spinal cord. Neuron 14:949–959.

Ming GL, Wong ST, Henley J, Yaun XB, Song HJ, Spitzer NC, Poo MM (2002) Adaptation in the chemotactic guidance of nerve growth cones. Nature 417:411–418.

Mitchell KJ, Doyle JL, Serafini T, Kennedy TE, Tessier-Lavigne M, Goodman CS, Dickson BJ (1996) Genetic analysis of Netrin genes in *Drosophila*: netrins guide CNS commissural axons and peripheral motor axons. Neuron 17:203–215.

Monschau B, Kremoser C, Ohta K, Tanaka H, Kaneko T, Yamada T, Handwerker C, Hornberger MR, Loschinger J, Pasquale EB, Siever DA, Verderame MF, Muller BK, Bonhoeffer F, Drescher U (1997) Shared and distinct functions of RAGS and ELF-1 in guiding retinal axons. EMBO 16:1258–1267.

Norbeck BA, Feng Y, Denburg JL (1992) Molecular gradients along the proximal-distal axis of embryonic insect legs: possible guidance cues of pioneer axon growth. Development 116:467–479.

O'Connor TP, Bentley D (1993) Accumulation of actin in subsets of pioneer growth cone filopodia in response to neural and epithelial guidance cues in situ. J Cell Biol 123:935–948.

O'Connor TP, Duerr JS, Bentley D (1990) Pioneer growth cone steering decisions mediated by single filopodial contacts *in vivo*. J Neurosci 10:3935–3946.

Parent CA, Devreotes PN (1999) A cell's sense of direction. Science 284:765–770.

Pini A (1993) Chemorepulsion of axons in the developing mammalian central nervous system. Science 261:95–98.

Ramon y Cajal S (1937) Recollections of my life. Philadelphia: American Philosophical Society.

Rosentreter SM, Davenport RW, Loschinger J, Huf J, Jung J, Bonhoeffer F (1998) Response of retinal ganglion cell axons to striped linear gradients of repellent guidance molecules. J Neurobiol 37:541–562.

Sasaki T, Irie-Sasaki J, Jones RG, Oliveira-dos-Santos AJ, Stanford WL, Bolon B, Wakeham A, Itie A, Bouchard D, Kozieradzki I, Joza N, Mak TW, Ohashi PS, Suzuki A, Penninger JM (2000) Function of PI3Kγ in thymocyte development, T cell activation, and neutrophil migration. Science 287:1040–1046.

Seaver EC, Carpenter EM, Bastiani MJ (1996) REGA-1 is a GPI-linked member of the immunoglobulin superfamily present on restricted regions of sheath cell processes in grasshopper. Development 122:567–578.

Serafini T, Colamarino SA, Leonardo ED, Wang H, Beddington R, Skarnes WC,Tessier-Lavigne M (1996) Netrin-1 is required for commissural axon guidance in the developing vertebrate nervous system. Cell 87:1001–1014.

Servant G, Weiner OD, Herzmark P, Balla T, Sedat JW, Bourne HR (2000) Polarization of chemoattractant receptor signaling during neutrophil chemotaxis. Science 287:1037–1040.

Tessier-Lavigne M, Placzek M, Lumsden AGS, Dodd J, Jessell TM (1988) Chemotropic guidance of developing axons in the mammalian central nervous system. Nature 336:775–778.

Walter J, Allsopp TE, Bonhoeffer FA (1990) A common denominator of growth cone guidance and collapse? Trends Neurosci 13:447–452.

Weiner OD, Servant G, Welch MD, Mitchison TJ, Sedat JW, Bourne HR (1999) Spatial control of actin polymerization during neutrophil chemotaxis. Nat Cell Biol 1:75–81.